ATLAS NOTE

ATLAS-CONF-2013-028

March 10, 2013
Minor Revision: April 24, 2013

Search for electroweak production of supersymmetric particles in final states with at least two hadronically decaying taus and missing transverse momentum with the ATLAS detector in proton-proton collisions at $\sqrt{s}$ = 8 TeV

The ATLAS Collaboration

Abstract

Results of a search for the production of weakly coupled supersymmetric particles decaying into final states with at least two hadronically decaying taus and missing transverse momentum are presented. The analysis uses the complete 2012 data sample of $\sqrt{s}$ = 8 TeV proton-proton collisions recorded with the ATLAS detector at the CERN Large Hadron Collider, corresponding to a total integrated luminosity of 20.7 fb^{-1}. No deviation from the Standard Model expectation is observed. Exclusion limits at 95% confidence level are derived in the context of the phenomenological Minimal Supersymmetric Standard Model and Simplified Models characterized by the presence of low mass staus. For Simplified Models, chargino masses up to 350 GeV are excluded for a massless lightest neutralino in the scenario of direct production of wino-like chargino pairs decaying into the lightest neutralino via an intermediate on-shell tau slepton. In the case of pair production of degenerate charginos and next-to-lightest neutralinos, masses up to 330 (300) GeV are excluded for lightest neutralino masses below 50 (100) GeV.

A typo has been found in the mass of $\tilde{\chi}_1^{\pm}$ of SUSY reference point 2 on page 3 in the version of March 10. None of the figures, tables or conclusion have been changed.

1 Introduction

One of the most appealing extensions to the Standard Model (SM) of particle physics is supersymmetry (SUSY) [1–9]. In R-parity conserving SUSY models [10–14], SUSY particles are produced in pairs and the Lightest Supersymmetric Particle (LSP) is stable and weakly interacting. From a theoretical point of view, beneficial features of SUSY models are that they could solve the hierarchy problem [14–19], as well as provide a dark matter candidate (the LSP) [20–22]. In several SUSY models, the mass eigenstates formed from the linear superposition of the SUSY partners of the charged and neutral Higgs and electroweak gauge bosons, charginos ($\tilde{\chi}_i^{\pm}$, i = 1, 2) and neutralinos ($\tilde{\chi}_j^0$, j = 1, 2, 3, 4), as well as sleptons (superpartners of leptons, $\tilde{\ell}$ and $\tilde{\nu}$) can be sufficiently light to be produced at the LHC.

In the search presented here, Simplified Models [23] based on $\tilde{\chi}_1^{\pm}\tilde{\chi}_2^0$ production and $\tilde{\chi}_1^{\pm}\tilde{\chi}_1^{\mp}$ production, where the charginos and neutralinos decay with 100% branching fraction to final states with (s)taus, are considered. A similar situation may also be realized in the framework of the phenomenological Minimal Supersymmetric Standard Model (MSSM), the pMSSM [24], where the dominant electroweak production channels are $\tilde{\chi}_1^{\pm}\tilde{\chi}_2^0$ and $\tilde{\chi}_1^{\pm}\tilde{\chi}_1^{\mp}$. Their decay properties depend on the MSSM parameters M_1 and M_2 (the gaugino masses), $\tan\beta$ (the ratio of the vacuum values of the two neutral Higgses), and μ (the higgsino mixing mass term) which enter the neutralino and chargino mixing matrices [25]. The results are therefore also interpreted in the context of the pMSSM, with parameters chosen to enhance (s)tau production. In all cases the lightest neutralino ($\tilde{\chi}_1^0$) is the LSP. The probed new physics signatures are (see Figures 1 and 2):

- chargino-neutralino production, $\tilde{\chi}_1^{\pm}\tilde{\chi}_2^0 \to \tilde{\tau}_L\nu(\tau\tilde{\nu})\ \tilde{\tau}_L\tau \to \tau\nu\tilde{\chi}_1^0\ \tau\tau\tilde{\chi}_1^0$;
- chargino-chargino production: $\tilde{\chi}_1^{\pm}\tilde{\chi}_1^{\mp} \to 2\times\tilde{\tau}\nu(\tilde{\nu}\tau) \to 2\times\tau\nu\tilde{\chi}_1^0$;
- direct tau slepton production: $\tilde{\tau}^{\pm}\tilde{\tau}^{\mp} \to 2\times\tau\tilde{\chi}_1^0$.

Previous results from the ATLAS Collaboration cover electroweak production of supersymmetric particles in final states with electrons and muons, using signal models where the neutralinos and charginos decay with equal probability to all lepton flavours [26–28]. Preliminary limits on the chargino and neutralino masses in tau dominated scenarios have recently been presented by the CMS collaboration [29].

Final states containing at least two hadronically decaying taus are considered in this search. At least one tau pair is required to have opposite sign (OS). Events with additional light leptons (electrons or muons) are vetoed to allow for a statistical combination with similar searches using light leptons. The main SM background processes contributing to the selected final states are multi-jet production and W bosons produced in association with jets. In the first case the two tau candidates are misidentified; in the second case, one tau is produced in the W boson decay, and the other candidate is a misidentified jet. The analysis exploits the expected large magnitude of the missing transverse momentum, $E_{\mathrm{T}}^{\mathrm{miss}}$, generated by undetected LSPs, to discriminate SM processes from SUSY signal events. A further discriminating variable used in this search is the "stransverse mass" reconstructed using the two hadronic taus and $E_{\mathrm{T}}^{\mathrm{miss}}$. The stransverse mass, m_{T2}, can be shown to have a kinematic endpoint for events where two massive pair-produced particles both decay to two objects, one of which is detected (the lepton in this case) and the other not (the neutralino) [30, 31]. In signal events, the kinematic endpoint depends on the mass difference between the decaying SUSY particle and the LSP.

2 SUSY models

We consider a pMSSM model with the following specifications. Squark and gluino masses are set to 3 TeV, $\tan\beta$ to 50, and M_1 to 50 GeV. M_2 and μ are varied between 100 and 500 GeV. The lightest stau mass

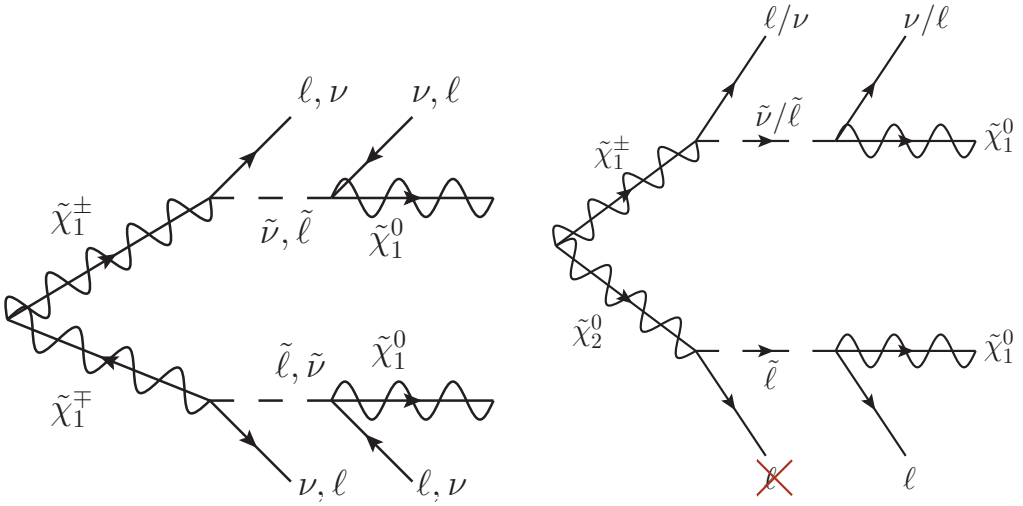

Figure 1: Feynman diagrams for $\tilde{\chi}_1^{\pm}\tilde{\chi}_1^{\mp}$ (left) and $\tilde{\chi}_2^0\tilde{\chi}_1^{\pm}$ (right) decays with intermediate light left-handed charged sleptons and sneutrinos. The $\tilde{\chi}_2^0\tilde{\chi}_1^{\pm}$decay yields either 3 hadronic taus in the final state, or two in the case where the third lepton is missed because it is not reconstructed or is out of the detector acceptance.

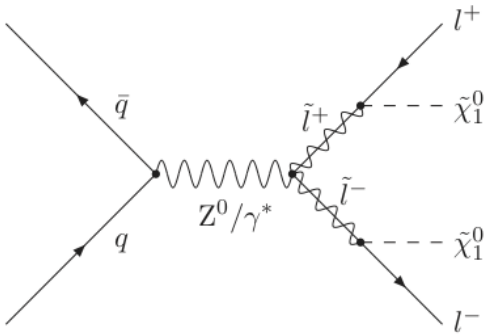

Figure 2: A Feynman diagram illustrating the pair production of charged sleptons and subsequent decay into a two-lepton final state. Only staus are considered throughout this document.

is set to 95 GeV (LEP limit) [32–35], and the other slepton masses are heavy. In the considered pMSSM scenario, the dominant production processes are direct stau production and pair production of neutralino-chargino or chargino-chargino. In the former case, staus decay directly to the lightest neutralino and a tau, resulting in a $\tau^+\tau^-+E_{\mathrm{T}}^{\mathrm{miss}}$ final state. In the latter case, the neutralinos and charginos will decay giving a variety of final states with multiple taus.

In addition, two Simplified Models are considered: neutralino-chargino ($\tilde{\chi}_1^{\pm}\tilde{\chi}_2^0$) and chargino-chargino ($\tilde{\chi}_1^{\pm}\tilde{\chi}_1^{\mp}$) production, where the neutralinos and charginos decay via intermediate charged sleptons and sneutrinos. All sparticles other than $\tilde{\chi}_1^{\pm}$, $\tilde{\chi}_2^0$, $\tilde{\chi}_1^0$, left-handed stau and tau sneutrino are assumed to be heavy. The stau and tau sneutrino are assumed to be mass degenerate, which is a fair assumption for large mass splitting between $\tilde{\chi}_1^{\pm}$ and $\tilde{\chi}_1^0$. Furthermore, $\tilde{\chi}_1^{\pm}$ and $\tilde{\chi}_2^0$ are assumed to be mass-degenerate without too much loss of generality. The $\tilde{\chi}_1^{\pm}$ mass is varied between 0 and 400 GeV, and the $\tilde{\chi}_1^0$ mass is varied between 0 and 250 GeV. The cross section for electroweak production of supersymmetric particles ranges between 10 and 0.01 pb in the considered models.

Two reference SUSY points are used throughout this document:

- SUSY Ref. point 1: chargino-neutralino production with mass($\tilde{\chi}_1^{\pm}, \tilde{\chi}_1^0$) = (250, 100) GeV;
- SUSY Ref. point 2: chargino-chargino production with mass($\tilde{\chi}_1^{\pm}, \tilde{\chi}_1^0$) = (250, 50) GeV.

A Simplified Model featuring only direct production of left-handed stau pairs is also considered, despite the low yields expected for this process. The cross section for direct stau production is one or two orders of magnitude lower than that of neutralinos and charginos and decreases from 0.2 to 0.03 pb as the stau mass increases from 80 to 140 GeV. The stau masses are generated in the range 80-140 GeV and the $\tilde{\chi}_1^0$ mass varies between 0 and 40 GeV. Masses of all neutralinos and charginos other than the lightest neutralino are set to 2.5 TeV.

3 Signal and background simulation

The main sources of SM background, multi-jet and W+jets events, are estimated with data-driven methods. Monte Carlo (MC) simulation is used to estimate the SUSY signal yields, as well as SM background contributions from processes leading to two real taus in the final state, such as top pair, single top and diboson (WW, WZ, ZZ) production, and Z boson production in association with jets. The SHERPA generator [36] is used for $t\bar{t}$, VV ($V = W, Z$) and Z+jets simulation. SHERPA MC samples of W boson production in association with jets are used as a cross check and for systematics studies. The W/Z+jets and $t\bar{t}$ samples contain matrix element (ME) calculations for up to four and five additional outgoing partons, respectively. The diboson samples use the default SHERPA settings for renormalization and factorization scales and are generated with a cut on the invariant mass of the lepton pairs, $m_{ll} > 0.4$ GeV. Samples of $t\bar{t}$+V ($V = W, Z$) are generated with MadGraph [37] interfaced to PYTHIA [38]. Single-top production is simulated with MC@NLO (Wt and s-channel) [39] and AcerMC (t-channel) [40]. The NLO CT10 [41] parton distribution function (PDF) set is used for SHERPA and MC@NLO. The CTEQ6L1 [42] set is used for MadGraph, AcerMC, PYTHIA. For the comparison with data, all SM background cross sections are normalized to the results of higher-order calculations when available. The theoretical cross sections for W+jets and Z+jets are calculated with DYNNLO [43] with the MSTW2008NNLO [44] PDF set. The inclusive $t\bar{t}$ cross section is calculated with HATHOR [45] using the MSTW2008NNLO PDFs. The production of dibosons [46] and $t\bar{t}$ in association with W/Z [47, 48] are normalized to NLO cross sections.

The SUSY signal samples are generated with HERWIG++ [49] and the CTEQ6L1 PDF. The mass spectra are calculated with ISASUSY 7.80 [50], and the cross-sections are calculated to next-to-leading order with PROSPINO [51].

MC samples are processed through a detailed detector simulation [52] based on Geant4 [53] and reconstructed in the same manner as the data. The effect of multiple pp collisions in the same bunch crossing (pile-up) is modeled by overlaying simulated minimum-bias events to the MC hard-scattering event, suitably reweighted to reproduce the distribution observed in data.

4 Event selection and reconstruction

The ATLAS experiment is a multi-purpose particle physics detector with forward-backward symmetric cylindrical geometry, and nearly 4π coverage in solid angle [54]. It features inner tracking detectors surrounded by a 2 T superconducting solenoid, electromagnetic and hadronic calorimeters, and a muon spectrometer consisting of precision-tracking and triggering chambers in a toroidal magnetic field.

The calorimeters, with acceptance covering the pseudorapidity[1] range $|\eta| < 4.9$, are composed of high-granularity liquid-argon calorimeters with lead, copper, or tungsten absorbers and an iron-scintillator calorimeter. Events are selected by a three level trigger system.

4.1 Object reconstruction

Jets are reconstructed from three-dimensional calorimeter energy clusters by the anti-k_t algorithm [55,56] with a radius parameter of 0.4. Jet energies are corrected [57] for detector inhomogeneities, the non-compensating nature of the calorimeter, and the impact of multiple overlapping pp interactions, using factors derived from test beam, cosmic ray, and pp collision data, and from a detailed `Geant4` detector simulation [52]. We distinguish between light central jets, forward jets, and b-jets. Light central jets are required to have transverse momentum $p_{\mathrm{T}} > 25$ GeV and $|\eta| < 2.5$. To efficiently reject jets originating from pile-up interactions, at least 20% of the scalar sum of the p_{T} of all tracks associated with the jet is required to come from tracks originating from the primary vertex of the event. The primary vertex of the event is required to be consistent with the beam spot envelope and to have at least 5 associated tracks; when more than one such vertex is found, the vertex with the largest summed $|p_{\mathrm{T}}|^2$ of the associated tracks is chosen. Forward jets must satisfy $p_{\mathrm{T}} > 30$ GeV and $2.5 < |\eta| < 4.5$. Jets originating from b-quarks (b-jets) are identified using information related to track impact parameters and reconstructed secondary vertices [58]. The b-tagging requirements are set to an operating point corresponding to an average efficiency of 80%. The b-jets are required to have $p_{\mathrm{T}} > 20$ GeV and $|\eta| < 2.5$.

The reconstruction of hadronically decaying taus is based on the information from topological clusters in the electromagnetic and hadronic calorimeters. The tau reconstruction algorithm is seeded by jets with $p_T > 10$ GeV and $|\eta| < 2.5$. Tracks are subsequently associated with the tau cluster within a cone of $\Delta R < 0.2$ around the axis of the seed jet. The reconstructed energy of the hadronic tau candidates is corrected to the tau energy scale, which is calibrated independently of the jet energy scale by a MC-based procedure [59]. Since the most common hadronic decays of taus are decays to either one or three charged pions, a neutrino and often additional neutral pions, taus are required to have 1 or 3 tracks (prongs) and a total charge of the tracks of either +1 or −1. For an improved discrimination between hadronically decaying taus and jets, electrons and muons, a multivariate algorithm is used [60]. The tau identification used in this analysis is based on the Boosted Decision Tree (BDT) method. A "jet BDT" is used to discriminate taus from jets, and an "electron BDT" to discriminate between electrons and taus. Based on the jet BDT result, we distinguish between three tau identification criteria, corresponding to "loose", "medium", and "tight" quality for the jet discrimination. These BDT identification for the jet discrimination have signal efficiencies of about 60%, 40% and 30%, respectively. The electron BDT discrimination is applied only to 1-prong taus, and the "loose" quality selection point is chosen. This requirement has about 95% signal efficiency. In addition, a dedicated muon veto is applied to remove tau candidates from muons coinciding with anomalous energy deposits in the calorimeter. Tau candidates are required to have $p_{\mathrm{T}} > 20$ GeV and $|\eta| < 2.5$.

Electron candidates must satisfy the "medium++" selection criteria [61] and are required to fullfill $p_{\mathrm{T}} > 10$ GeV, $|\eta| < 2.47$. Muon candidates are identified by matching an extrapolated inner detector track and one or more track segments in the muon spectrometer [62, 63]. They are required to fulfill $p_{\mathrm{T}} > 10$ GeV, $|\eta| < 2.4$.

The calculation of $E_{\mathrm{T}}^{\mathrm{miss}}$ [64] is based on the vectorial sum of the p_{T} of reconstructed objects (jets, leptons, photons) as well as calorimeter energy clusters (with $|\eta| < 4.9$) not belonging to reconstructed objects.

[1]The pseudorapidity is defined in terms of the polar angle θ as $\eta = -\ln\tan(\theta/2)$ and the rapidity is defined as $y = \ln[(E+p_z)/(E-p_z)]/2$. The separation between final state particles is defined as $\Delta R = \sqrt{(\Delta y)^2 + (\Delta\phi)^2}$ and is Lorentz invariant under boosts along the z-axis. The transverse momentum is denoted as p_{T}.

The overlap between the various reconstructed objects is resolved as follows. Jet candidates are removed if they lie within a distance $\Delta R = \sqrt{(\Delta\eta)^2 + (\Delta\phi)^2} < 0.2$ of a tau or an electron. The remaining electron and muon candidates are rejected if they lie within $0.2 < \Delta R < 0.4$ of a jet. Electron and muon candidates closer than $\Delta R = 0.1$, or muon candidates closer than $\Delta R = 0.05$, are rejected. To remove low mass resonances, pairs of opposite sign and same flavour leptons are rejected if their invariant mass is less than 12 GeV. Any tau candidate lying within a distance $\Delta R < 0.2$ of any remaining electron or muon is discarded.

4.2 Event selection

In order to maximize the efficiency for SUSY signal events a combination of a di-tau trigger and a trigger on missing transverse momentum is used. Trigger efficiency studies show that the di-tau trigger reaches its efficiency plateau (at about 65% efficiency) when the leading tau has $p_{\mathrm{T}} > 40$ GeV and the next-to-leading tau has $p_{\mathrm{T}} > 25$ GeV. The $E_{\mathrm{T}}^{\mathrm{miss}}$ trigger is fully efficient for events with $E_{\mathrm{T}}^{\mathrm{miss}}$ above 150 GeV. Events where the taus have $p_{\mathrm{T}} > 20$ GeV but the di-tau trigger has not fired are recovered by the $E_{\mathrm{T}}^{\mathrm{miss}}$ trigger. Due to the large $E_{\mathrm{T}}^{\mathrm{miss}}$ requirement, however, this trigger only contributes a small fraction of the signal acceptance.

The event preselection requires the di-tau and/or $E_{\mathrm{T}}^{\mathrm{miss}}$-based trigger to have fired. Events with at least two taus of medium quality for the jet discrimination are selected, and one of these must satisfy the tight quality requirement. At least one of the selected tau pairs must be oppositely charged. Events with additional light leptons are vetoed.

To reject Z+jets events, events where the visible invariant mass of at least one of the oppositely charged tau pairs is within 10 GeV of the fitted value of the visible Z boson mass (81 GeV) obtained from a MC $Z(\rightarrow \tau\tau)$+jets sample are vetoed. This requirement on the visible di-tau mass is referred to as the "Z-veto".

At tree level, no jet is present in the processes of interest shown in Figures 1 and 2. However, jets can be generated from initial state radiation (ISR). To reduce backgrounds with top quarks but allow for ISR, either an event-based jet veto, rejecting events containing light central jets, forward jets or b-jets, or a b-jet veto only, rejecting events containing b-jets, is applied. Both requirements are powerful in rejecting backgrounds containing top quarks. The rejection of the (b-)jet veto on top backgrounds ($t\bar{t}$, single top and $t\bar{t}$+V) is about (10) 100. The trigger efficiency on selected events passing all the analysis cuts is around 90% for SUSY Ref point 1 and 2.

4.3 Signal regions

To further improve the signal over background ratio, requirements on $E_{\mathrm{T}}^{\mathrm{miss}}$ and m_{T2} are applied. In events where more than two taus are selected, m_{T2} is computed among all possible OS tau pairs and the largest value is chosen.

The signal region definition has been optimized on the SUSY models described in Section 2. Two signal regions are defined (see also Table 1 for a detailed specification of the selection requirements):

- **SR OS-m_{T2}**: A jet veto is applied. Events are required to have $E_{\mathrm{T}}^{\mathrm{miss}} > 40$ GeV and $m_{\mathrm{T2}} > 90$ GeV;
- **SR OS-m_{T2}-nobjet**: A b-jet veto is applied. Events are required to have $E_{\mathrm{T}}^{\mathrm{miss}} > 40$ GeV and $m_{\mathrm{T2}} > 100$ GeV.

Signal region	requirements
OS m_{T2}	at least 1 OS tau pair
	jet veto
	Z-veto
	$E_{\mathrm{T}}^{\mathrm{miss}}$> 40 GeV
	m_{T2}> 90 GeV
OS m_{T2}-nobjet	at least 1 OS tau pair
	b-jet veto
	Z-veto
	$E_{\mathrm{T}}^{\mathrm{miss}}$> 40 GeV
	m_{T2}> 100 GeV

Table 1: Definition of the signal regions.

5 SM Background determination

Two types of SM backgrounds are considered, according to the origin of the tau: fake taus from mis-identified jets (the contribution of real taus from heavy-flavour decays in jets is negligible) and real taus from prompt boson decays.

The reducible background consists of events containing one or more fake taus, primarily multi-jet and W+jets events. The irreducible background consists of events containing real taus. These include diboson, Z+jets or top production ($t\bar{t}$, single top and $t\bar{t}$+V). There may be contributions from fake taus also in these processes, however these are subdominant with respect to the real tau contribution. The contribution from real taus exceeds 90% in Z+jets and diboson production, and ranges from 45% to 75% in backgrounds containing top quarks.

5.1 Reducible background estimation

The dominant background in the SRs originates from fake taus (75-80%). The fake tau rate modelling in the MC is not accurate. Moreover the available MC samples for both multi-jet and W+jets production are insufficient to provide a precise estimate of these contributions. The latter are therefore derived from data using the "ABCD" method.

Four exclusive regions, labelled as A, B, C (the control regions) and D (the SR), are selected in a plane defined by two weakly correlated variables. For uncorrelated variables, the ratio of the numbers of events in the control regions A and B equals that of SR D to control region C: the number of events in the SR D, N_D, can therefore be calculated from that in control region A, N_A, multiplied by a normalization factor N_C/N_B.

The tau identification criterion (tau-id) and m_{T2} are chosen as discriminating variables to define the regions A, B, C and D. The control and signal regions are defined in the same way except that in the A and B control regions we require taus satisfying a "loose" but failing "tight" selection criteria (tight veto), which is orthogonal to the signal region criterion. In control regions B and C we require furthermore $m_{\mathrm{T2}} < 40$ GeV. In the signal regions at least one tight tau and one medium tau are required, and $m_{\mathrm{T2}} > 90$ GeV for SR OS-m_{T2} ($m_{\mathrm{T2}} > 100$ GeV for SR OS-m_{T2}-nobjet). The main contribution to the CRs comes from by multi-jet and W+jets events ($\geq 90\%$). The W+jets contribution in the CRs ranges from 2% to 10%. Contributions from other SM processes are small and subtracted using the MC simulation. The definitions of the control and signal regions are summarized in Table 2. Furthermore two validation regions E and F are defined. The validation region E (F) has the same definition as the control region A

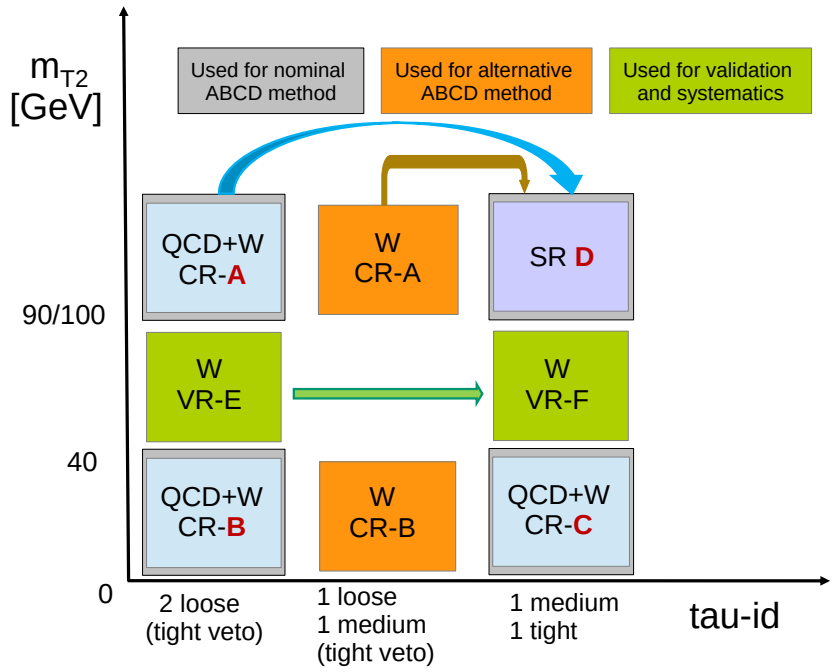

Figure 3: Illustration of the ABCD method for the inclusive multi-jet and W+jets background determination. The control regions B, C, A, D for the nominal ABCD method described in the text (labelled as QCD+W CR-B/C/A and SR D) are drawn as light blue boxes. Shown in green and labelled as W-VR are the regions E (same as QCD+W CR-B except for requiring $40 < m_{T2} < 90$ GeV) and F (same as QCD+W CR-C except for requiring $40 < m_{T2} < 90$ GeV), which are used to validate the ABCD method and to estimate the systematic uncertainties. The nominal ABCD method is cross-checked by varying the composition of the CRs. The regions labelled as W CR-A, W CR-B are the ones used for the cross-check and are shown in orange.

(signal region D) except for requiring $40 < m_{T2} < 90$ GeV. The validation regions E and F are richer in W+jets events than control regions B and C, and are used to verify the ABCD method and to estimate the systematic uncertainty from the residual correlation between tau-id and m_{T2}. The regions A – F are drawn schematically in Figure 3.

The m_{T2} distributions in the control and validation regions are shown in Figure 4. The results of the ABCD method are summarized in Table 3. The impact of a possible contamination in the control regions has been tested using various signal models (also reported in Table 3). It has been found to be small compared to the total uncertainty in the multi-jet and W+jets background predictions.

The multi-jet and W+jets background estimation has been validated with an alternative ABCD method using control regions with different background composition, i.e. richer in W+jets events than the CRs A and B (the W-CRs A and B in Figure 4), and consistent results have been obtained.

5.2 Irreducible background estimation

Irreducible SM backgrounds arise mainly from $t\bar{t}$, single top, $t\bar{t}+V$, Z/γ^*+jets and diboson (WW, WZ and ZZ) processes and are estimated from MC simulation. The simulation is corrected for the difference in efficiency of the tau identification and trigger between data and MC for both real and fake taus. The correction is calculated with a Tag-and-Probe method in a sample of $Z \to \tau\tau \to \mu\tau_{had}$ events for real taus and $W \to \mu\nu$ events for fake taus.

Regions	multi-jet and W+jets background control region			Signal region
	A	B	C	D
OS m_{T2}	m_{T2}> 90 GeV $E_{\mathrm{T}}^{\mathrm{miss}}$> 40 GeV ≥ 2 loose taus tight tau veto	m_{T2}< 40 GeV $E_{\mathrm{T}}^{\mathrm{miss}}$> 40 GeV ≥ 2 loose taus tight tau veto	m_{T2}< 40 GeV $E_{\mathrm{T}}^{\mathrm{miss}}$> 40 GeV ≥ 1 medium tau ≥ 1 tight tau	m_{T2}> 90 GeV $E_{\mathrm{T}}^{\mathrm{miss}}$> 40 GeV ≥ 1 medium tau ≥ 1 tight tau
OS m_{T2}-nobjet	m_{T2}> 100 GeV $E_{\mathrm{T}}^{\mathrm{miss}}$> 40 GeV ≥ 2 loose taus tight tau veto	m_{T2}< 40 GeV $E_{\mathrm{T}}^{\mathrm{miss}}$> 40 GeV ≥ 2 loose taus tight tau veto	m_{T2}< 40 GeV $E_{\mathrm{T}}^{\mathrm{miss}}$> 40 GeV ≥ 1 medium tau ≥ 1 tight tau	m_{T2}> 100 GeV $E_{\mathrm{T}}^{\mathrm{miss}}$> 40 GeV ≥ 1 medium tau ≥ 1 tight tau

Table 2: The signal and the multi-jet and W+jets background control region definitions.

		region A	region B	region C	region E	region F	transfer factor	multi-jet and W+jets in SR
OS m_{T2}	Data	12	26932	22382	2781	2270	0.760 ±0.010	8.4 ±3.0
	Z+jets	-	(3.7 ± 0.6) ×10^2	(2.13 ± 0.19) ×10^3	40±23	68±21		
	di-boson	0.84±0.22	6.6±0.8	23.1±1.3	4.8±0.7	15.8±1.2		
	single top	-	0.21±0.21	3.1±1.9	1.7±1.1	1.1±0.5		
	$t\bar{t}$	0.13±0.13	0.31±0.20	2.0±0.7	1.0±0.4	1.2±0.4		
	Drell-Yan	-	0.7±0.7	43±25	-	-		
	Multi-jet, W+jets	11.0±3.5	(2.655 ± 0.018) ×10^4	(2.018 ± 0.024) ×10^4	(2.73 ± 0.06) ×10^3	2.08 ± 0.04 ×10^3		
	Ref. Point 1	1.5 ±0.5	0.6±0.3	2.4±0.6	2.9±1.4	12.4±1.5		
	Ref. Point 2	2.2±0.4	1.9±0.4	11.5±1.1	3.4±0.5	20.0±1.1		
OS m_{T2} -nobjet	Data	18	41372	36291	10652	8597	0.782 ±0.008	12 ±5
	Z+jets	-	(9.0 ± 1.0) ×10^2	(4.47 ± 0.21) ×10^3	56±24	175±29		
	di-boson	0.98±0.23	13.6±1.1	52.2±2.0	8.9±0.9	26.8±1.4		
	single top	-	6.8±2.5	21±4	4.8±1.5	6.4±1.8		
	$t\bar{t}$	1.3±0.6	26.3±2.8	51.6±3.5	13.6±2.0	23.5±2.4		
	Drell-Yan	-	9±5	89±30	2.1 ±1.3	2.1±2.1		
	Multi-jet, W+jets	16±4	(4.042 ± 0.022) ×10^4	(3.160 ± 0.029) ×10^4	(1.057 ± 0.011) ×10^3	(8.26 ± 0.08) ×10^3		
	Ref. Point 1	2.0±0.6	1.2±0.4	13.3±0.2	5.3±1.5	29.7±2.2		
	Ref. Point 2	2.6±0.4	4.1±0.5	22.8±1.4	6.9±0.7	36.3±1.5		

Table 3: The expected backgrounds in each multi-jet and W+jets background control region and validation region and the estimate of the multi-jet and W+jets background contribution in the signal regions. The uncertainty in the last column is the total uncertainty on the multi-jet and W+jets background estimate, including both statistical and systematic uncertainties.

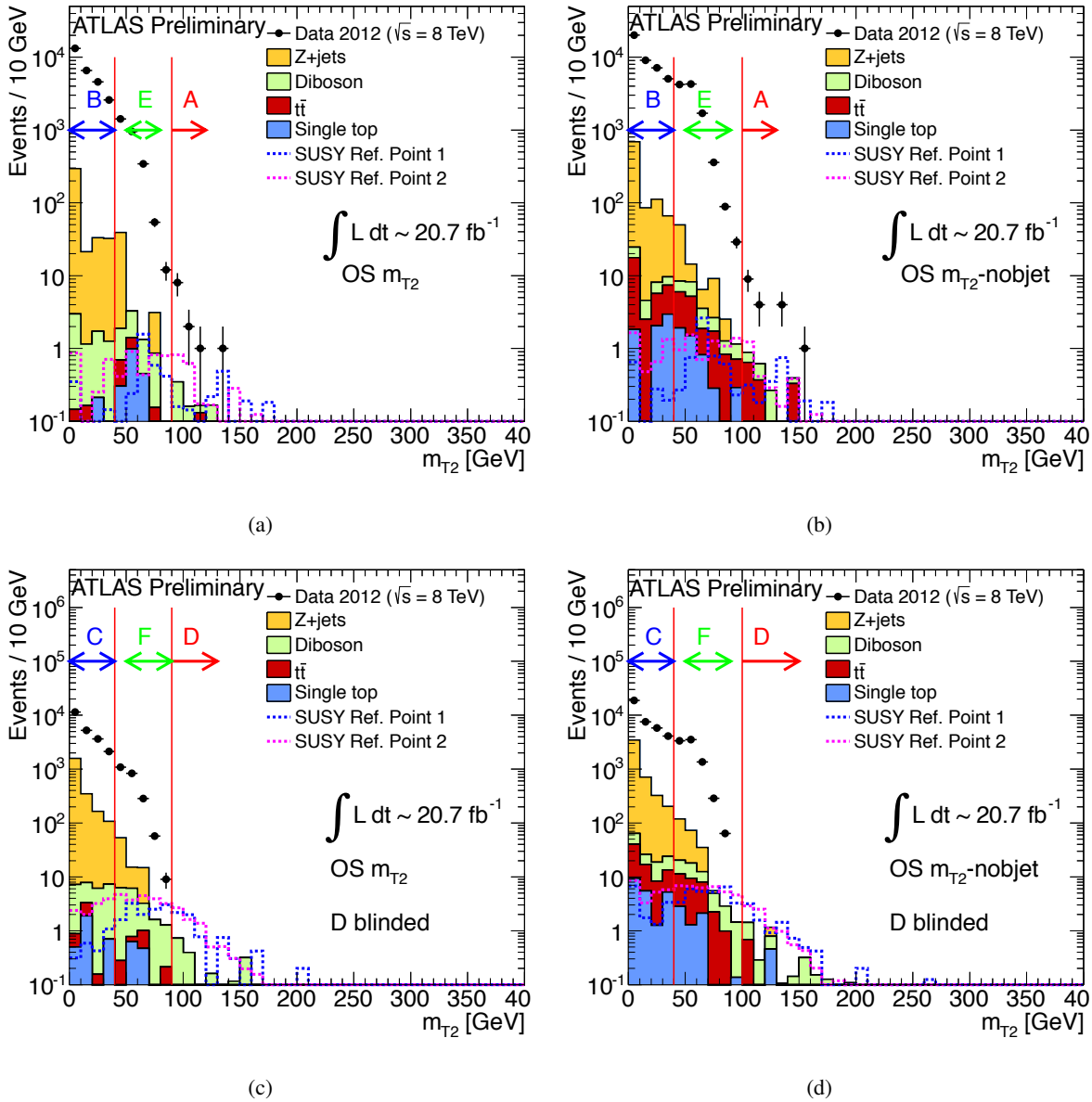

Figure 4: m_{T2} distribution after requiring at least two loose but not tight taus in the multi-jet and W+jets background CRs corresponding to (a) SR OS-m_{T2} and (b) SR OS-m_{T2}-nobjet, and after requiring at least one tight and one medium tau for (c) SR OS-m_{T2} and (d) SR OS-m_{T2}-nobjet. The stacked histograms show the contribution of the irreducible background from MC simulation, normalized to 20.7 fb^{-1}. The data points show that the background is dominated by multi-jet and W+jets production. Indicated in the plots are the control (A,B,C) and validation (E,F) regions. Data events in the signal region D are not shown.

The inclusive contribution from $t\bar{t}$, single top, $t\bar{t}$+V and Z/γ^*+jets amounts to about 1% of the total background in SR OS-m_{T2} and to about 10% in SR OS-m_{T2}-nobjet. The diboson background accounts for 20% in SR OS-m_{T2} and 15% in SR OS-m_{T2}-nobjet respectively. The main contribution from diboson production is given by $ZZ \to \tau\tau\nu\nu$ events. Other SM backgrounds are negligible.

The MC estimates, together with the prediction of the ABCD method, have been validated in regions enriched in W/Z+jets and $t\bar{t}$ events.

6 Systematic Uncertainties

Several sources of systematic uncertainty are considered for the ABCD method used to determine the reducible background. The correlation between the tau-id and m_{T2} variables for the multi-jet and W+jets backgrounds is estimated from the intermediate validation regions E and F. The transfer factor is defined as the ratio between the number of events in the loose tau-id regions (A, B) and the number of events in the medium+tight tau-id regions (D, C). Due to the small fraction of W+jets background events in the control regions, the transfer factor is dominated by multi-jet events. The transfer factor from the multi-jet dominated regions B and C is used, and the difference with the transfer factor calculated for W+jets events is treated as systematic uncertainty. The systematic uncertainty is obtained from the difference between the nominal ABCD transfer factor and that obtained using a W+jets MC sample. Other sources of systematic uncertainty arise from the subtraction of the irreducible background in region A (in regions B and C this background is negligible) and from the number of events in this region. The systematic uncertainties on the fake tau background estimation are summarized in Table 4. They are dominated by the limited statistics in the multi-jet and W+jets background control regions and by the transfer factor difference between multi-jet and W+jets background events.

Syst. Sources	SR OS-m_{T2}	SR OS-m_{T2}-nobjet
Correlation	5%	1%
Transfer factor difference	15%	24%
Subtraction of other backgrounds	2%	6%
Number of events in Region A	31%	27%
Total	35%	37%

Table 4: Summary of systematic uncertainties on the fake tau background estimation.

The following systematic uncertainties on the irreducible background have been considered: jet energy scale and resolution [57], $E_{\mathrm{T}}^{\mathrm{miss}}$ energy scale and resolution [64], and tau identification and trigger efficiencies and energy scale [59]. The main contribution comes from the tau-related systematic uncertainties, which are of the order of 5-30% for Z+jets, 5-15% for diboson production, and 30% for $t\bar{t}$, single top and $t\bar{t}$+V. Systematic uncertainties due to the choice of the MC generator have been evaluated by comparing the baseline estimates to those obtained with the following generators: HERWIG [65] for diboson, ALPGEN [66] for Z+jets, and POWHEG [67] for $t\bar{t}$ production. The resulting uncertainties are of the order of 10-30% for diboson, 40-50% for Z+jets, and 30-40% for $t\bar{t}$ production. A systematic uncertainty of the order of 10% associated with the simulation of pile-up is also taken into account. The luminosity uncertainty is 3.6% [68]. The theoretical uncertainties on the cross-sections are 5% for Z+jets [69], $^{+9.2}_{-10.1}$% for $t\bar{t}$, $^{+4.07}_{-2.69}$%, $^{+4.32}_{-3.89}$% and $^{+7.43}_{-7.69}$% for single top in the t-, s- and Wt- channels respectively, and 5%, 5% and 7% for WW, ZZ and WZ, respectively [70].

The total systematic uncertainty on the diboson background is around 30-40%, whereas for $t\bar{t}$, single top, $t\bar{t}$+V and Z+jets, it is around 70%. For signal events, the above sources of systematic uncertainties lead to a total systematic uncertainty of 15-20%.

7 Results and interpretations

The SM background estimates together with the observed data for each signal region are given in Table 5. Good agreement is found. The observed and expected numbers of events together with their uncertainties are used to calculate exclusion limits for the SUSY models described in Section 2.

Figure 5 shows the m_{T2} distribution for data and SM backgrounds in SR OS-m_{T2} and SR OS-m_{T2}-nobjet. The SM background distributions are taken from MC, except for the multi-jet and W+jets contribution, which is estimated using the ABCD method.

SM process	SR OS m_{T2}	SR OS m_{T2} -nobjet
top	0.2 ± 0.5 ± 0.1	1.6 ± 0.8 ± 1.2
Z+jets	0.28 ± 0.26 ± 0.23	0.4 ± 0.3 ± 0.3
diboson	2.2 ± 0.5 ± 0.5	2.5 ± 0.5 ± 0.9
multi-jet & W+jets	8.4 ± 2.6 ± 1.4	12 ± 3 ± 3
SM total	11.0 ± 2.7 ± 1.5	17 ± 4 ± 3
data	6	14
SUSY Ref. point 1	6.8 ± 1.0	9.2 ± 1.2
SUSY Ref. point 2	7.5 ± 0.7	8.9 ± 0.7

Table 5: Expected number of events from SM processes in the signal regions, normalized to 20.7 fb^{-1}, and the number of events observed in data. The first (second) uncertainty in each case is the statistical (systematic) uncertainty. The "top" contribution includes the single top, $t\bar{t}$, and $t\bar{t}$+V processes. The expected event yields for the two SUSY reference points are also shown.

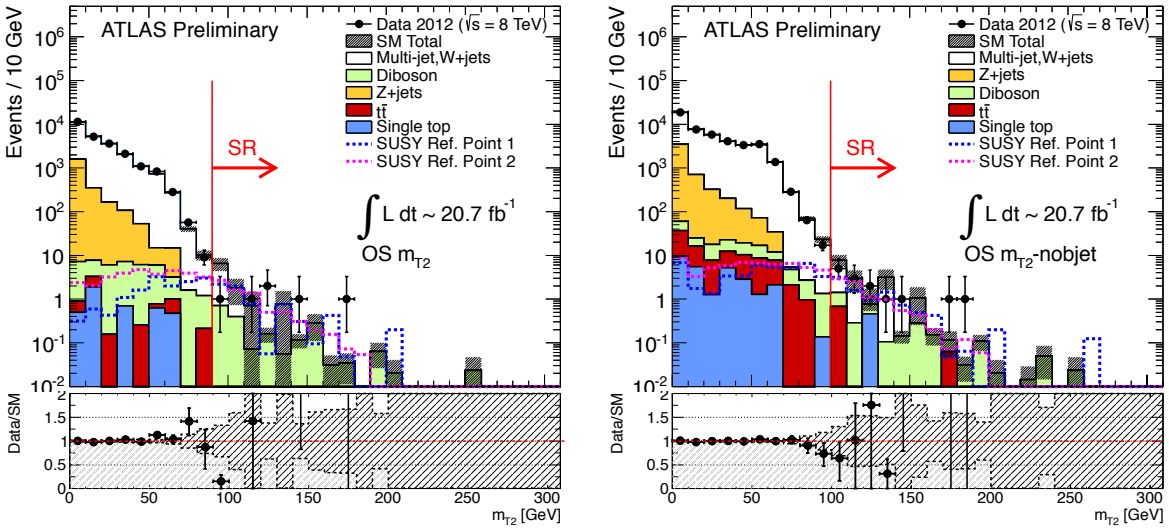

(a) SR OS-m_{T2}

(b) SR OS-m_{T2}-nobjet

Figure 5: m_{T2} distribution for (a) SR OS-m_{T2} and (b) SR OS-m_{T2}-nobjet. The stacked histograms show the expected backgrounds. The white histogram represents the multi-jet and W+jets contribution obtained from data using the ABCD method. The SM backgrounds are normalized to 20.7 fb^{-1}. The lower plots show the distributions of data over SM backgroud ratio.

The observed numbers of events in the signal regions are used to place model-independent upper limits at 95% confidence level (CL) on the visible cross-section. In addition, model-dependent exclusion limits at 95% CL are provided for the pMSSM and the Simplified Models described in Section 2. The exclusion limits are calculated using the CL_s prescription [71] by comparing the number of observed events in data with the SM expectation using the profile likelihood ratio as test statistic. All systematic uncertainties are taken into account via nuisance parameters.

Signal Region	$\langle\epsilon\sigma\rangle^{95}_{\text{obs}}$[fb]	S^{95}_{obs}	S^{95}_{exp}	CL_B	$p(s=0)$
SR-OSm_{T2}	0.27	5.6	$8.9^{+2.7}_{-3.2}$	0.14	0.42
SR-OSm_{T2}-nobjet	0.50	10.4	$10.4^{+0.6}_{-1.7}$	0.48	0.39

Table 6: Left to right: 95% CL upper limits on the visible cross section ($\langle\epsilon\sigma\rangle^{95}_{\text{obs}}$) and on the number of signal events (S^{95}_{obs}). The third column (S^{95}_{exp}) shows the expected 95% CL upper limit on the number of signal events, determined by using the expected background contribution. The last two columns indicate the confidence level for the background-only hypothesis (CL_B) and the compatibility of the data with the background-only expectation ($p(s=0)$).

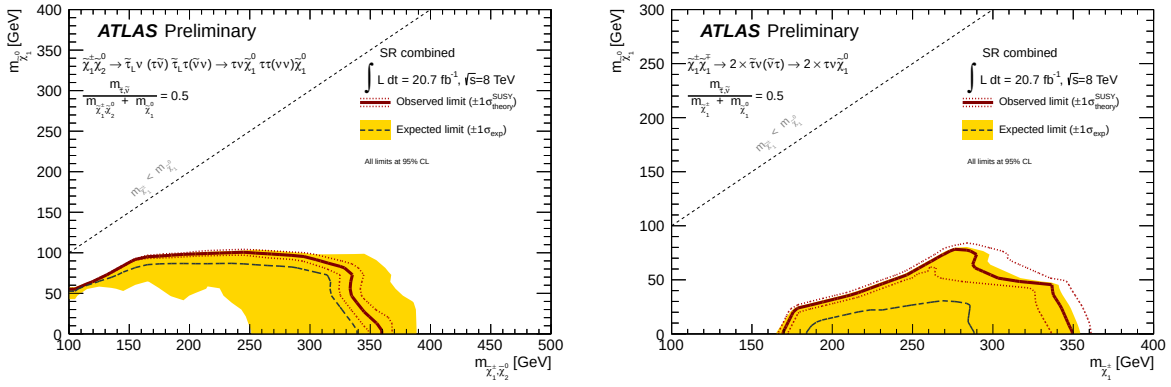

(a) (b)

Figure 6: 95% CL exclusion limits for Simplified Models with (a) chargino-neutralino and (b) chargino-chargino production. The SR with the best expected limit at each point is used. The dashed lines show the 95% CL expected limits. The solid band around the expected limit shows the $\pm1\sigma$ result where all uncertainties, except those on the signal cross-sections, are considered. The $\pm1\sigma$ lines around the observed limit represent the results obtained when moving the nominal signal cross-section up and down by the $\pm1\sigma$ theoretical SUSY signal uncertainty.

7.1 Model-independent upper limits

Model-independent upper limits at 95% CL are placed on the visible cross section of new physics processes defined as $\sigma_{vis} = \sigma \times \epsilon$, where ϵ is the acceptance $\times$ efficiency. Results are shown in Table 6.

7.2 Simplified Models: chargino-neutralino and chargino-chargino production

The observed and expected numbers of events in the signal regions are used to place limits in the ($m(\tilde{\chi}^{\pm}_1)$, $m(\tilde{\chi}^0_1)$) parameter space for the Simplified Model with chargino-neutralino production and the Simplified Model with chargino-chargino production with intermediate staus. The corresponding exclusion limits are shown in Figure 6. For each point in parameter space, the SR with the best expected limit is used.

Chargino masses up to 350 GeV are excluded for a massless lightest neutralino in the scenario of direct production of chargino pairs. In the case of pair production of degenerate charginos and next-to-lightest neutralinos, masses up to 330 (300) GeV are excluded for lightest neutralino masses below 50 (100) GeV.

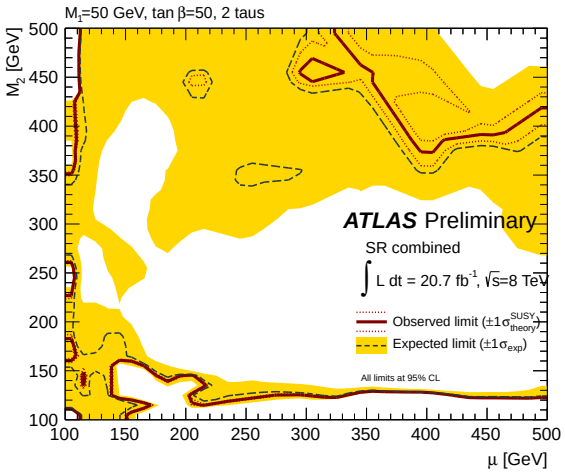

Figure 7: 95% CL exclusion limits in the μ-M_2 mass plane of the pMSSM with M_1=50 GeV, tanβ=50. The SR with the best expected limit at each point is used. The dashed lines show the 95% CL expected limits. The solid band around the expected limit shows the $\pm 1\sigma$ result where all uncertainties, except those on the signal cross-sections, are considered. The $\pm 1\sigma$ lines around the observed limit represent the results obtained when moving the nominal signal cross-section up and down by the $\pm 1\sigma$ theoretical SUSY signal uncertainty.

7.3 The pMSSM model

Limits on the neutralino and chargino mass parameters M_2 and μ are set within the pMSSM framework with parameters described in Section 2. Figure 7 shows the exclusion limits in the pMSSM μ-M_2 plane with M_1 equal to 50 GeV and tanβ equal to 50. The region at low M_2 can not be excluded since it corresponds to points in the parameter space where the chargino and neutralino are lighter than the stau. The region at large M_2 and μ corresponds to direct stau production.

7.4 Direct stau production

Due to the low cross-section compared to electroweak production, the analysis has low sensitivity to the direct production of tau sleptons. The best upper limit on the production cross-section is found for a stau mass of 140 GeV and a $\tilde{\chi}_1^0$ mass of 10 GeV. The theoretical cross section at NLO is 0.04 pb, and the excluded cross section is 0.17 pb.

8 Conclusions

A search for electroweak production of supersymmetric particles with at least two hadronically decaying taus in the final state has been presented. Good agreement between data and SM expectations is observed in all signal regions. These results are used to set limits on the visible cross section for signal-like events in each signal region. Exclusion limits, which extend the results of previous searches [29], are placed on the parameters of the pMSSM and Simplified Models.

For Simplified Models, chargino masses up to 350 GeV are excluded for a massless lightest neutralino in the scenario of direct production of wino-like chargino pairs decaying into the lightest neutralino via an intermediate on-shell tau slepton. In the case of pair production of degenerate charginos and next-to-lightest neutralinos, masses up to 330 (300) GeV are excluded for lightest neutralino masses below 50 (100) GeV.

References

[1] H. Miyazawa, *Baryon Number Changing Currents*, Prog. Theor. Phys. **36 (6)** (1966) 1266–1276.

[2] P. Ramond, *Dual Theory for Free Fermions*, Phys. Rev. **D3** (1971) 2415–2418.

[3] Y. A. Golfand and E. P. Likhtman, *Extension of the Algebra of Poincare Group Generators and Violation of p Invariance*, JETP Lett. **13** (1971) 323–326.

[4] A. Neveu and J. H. Schwarz, *Factorizable dual model of pions*, Nucl. Phys. **B31** (1971) 86–112.

[5] A. Neveu and J. H. Schwarz, *Quark Model of Dual Pions*, Phys. Rev. **D4** (1971) 1109–1111.

[6] J. Gervais and B. Sakita, *Field theory interpretation of supergauges in dual models*, Nucl. Phys. **B34** (1971) 632–639.

[7] D. V. Volkov and V. P. Akulov, *Is the Neutrino a Goldstone Particle?*, Phys. Lett. **B46** (1973) 109–110.

[8] J. Wess and B. Zumino, *A Lagrangian Model Invariant Under Supergauge Transformations*, Phys. Lett. **B49** (1974) 52.

[9] J. Wess and B. Zumino, *Supergauge Transformations in Four-Dimensions*, Nucl. Phys. **B70** (1974) 39–50.

[10] P. Fayet, *Supersymmetry and Weak, Electromagnetic and Strong Interactions*, Phys. Lett. **B64** (1976) 159.

[11] P. Fayet, *Spontaneously Broken Supersymmetric Theories of Weak, Electromagnetic and Strong Interactions*, Phys. Lett. **B69** (1977) 489.

[12] G. R. Farrar and P. Fayet, *Phenomenology of the Production, Decay, and Detection of New Hadronic States Associated with Supersymmetry*, Phys. Lett. **B76** (1978) 575–579.

[13] P. Fayet, *Relations Between the Masses of the Superpartners of Leptons and Quarks, the Goldstino Couplings and the Neutral Currents*, Phys. Lett. **B84** (1979) 416.

[14] S. Dimopoulos and H. Georgi, *Softly Broken Supersymmetry and SU(5)*, Nucl. Phys. **B193** (1981) 150.

[15] E. Witten, *Dynamical Breaking of Supersymmetry*, Nucl. Phys. **B188** (1981) 513.

[16] M. Dine, W. Fischler, and M. Srednicki, *Supersymmetric Technicolor*, Nucl. Phys. **B189** (1981) 575–593.

[17] S. Dimopoulos and S. Raby, *Supercolor*, Nucl. Phys. **B192** (1981) 353.

[18] N. Sakai, *Naturalness in Supersymmetric Guts*, Zeit. Phys. **C11** (1981) 153.

[19] R. Kaul and P. Majumdar, *Cancellation of quadratically divergent mass corrections in gobally supersymmetric spontaneously broken gauge theories*, Nucl. Phys. **B199** (1982) 36.

[20] G. Jungman, M. Kamionkowski, and K. Griest, *Supersymmetric Dark Matter*, Physics Reports **267** (1996) 195–373.

[21] H. Goldberg, *Constraint on the photino mass from cosmology*, Phys. Rev. Lett. **50** (1983) 1419.

[22] J. Ellis, J. Hagelin, D. Nanopoulos, K. Olive, and M. Srednicki, *Supersymmetric relics from the big bang*, Nucl. Phys. **B238** (1984) 453–476.

[23] P. S. J. Alwall and N. Toro, *Simplified Models for a First Characterization of New Physics at the LHC*, Phys Rev **D79** (2009) 075020.

[24] A. Djouadi, J-L. Kneur and G. Moultaka, *SuSpect: a Fortran Code for the Supersymmetric and Higgs Particle Spectrum in the MSSM*, Comput.Phys.Commun.**176**:426-455 (2007) [hep-ph/0211331]; C. F. Berger, J. S. Gainer, J. L. Hewett, T. G. Rizzo, *Supersymmetry Without Prejudice*, JHEP **0902** (2009) 023. [arXiv:0812.0980 [hep-ph]]; S. S. Abdus Salam, B. C. Allanach, F. Quevedo, F. Feroz and M. Hobson, *Fitting the Phenomenological MSSM*, Phys. Rev. **D 81** (2010) 095012 [arXiv:0904.2548 [hep-ph]] .

[25] K. Nakamura et al., *Review of Particle Physics*, J. Phys. G **37 075021** (2010) .

[26] ATLAS Collaboration, *Search for direct production of charginos and neutralinos in events with three leptons and missing transverse momentum in 13 fb^{-1} of pp collisions at $\sqrt{s}$ = 8 TeV with the ATLAS detector*, ATLAS-CONF-2012-154. `http://cdsweb.cern.ch/record/1398198`.

[27] ATLAS Collaboration, *Search for direct production of charginos and neutralinos in events with three leptons and missing transverse momentum in pp collisions with the ATLAS detector*, Physics Letters B **718** (2013) 841–859, `arXiv:1208.3144 [hep-ph]`.

[28] ATLAS Collaboration, *Search for direct slepton and gaugino production in final states with two leptons and missing transverse momentum with the ATLAS detector in pp collisions*, Physics Letters B **718** (2013) 879–901, `arXiv:1208.2884 [hep-ph]`.

[29] CMS Collaboration, *Search for electroweak production of charginos, neutralinos, and sleptons using leptonic final states in pp collisions at $\sqrt{s}$ = 8 TeV*, CMS-PAS-SUS-12-022. `http://cdsweb.cern.ch/record/1496092`.

[30] C. G. Lester and D. J. Summers, *Measuring masses of semiinvisibly decaying particles pair produced at hadron colliders*, Phys. Lett. **B463** (1999) 99–103, `arXiv:hep-ph/9906349`.

[31] A. Barr, C. Lester, and P. Stephens, *m(T2) : The Truth behind the glamour*, J. Phys. **G29** (2003) 2343–2363, `arXiv:hep-ph/0304226`.

[32] ALEPH Collaboration, *Search for scalar leptons in e^+e^- collisions at center-of-mass energies up to 209 GeV*, Phys.Lett. B **526** (2002) 206–220, `arXiv:hep-ph/0112011`.

[33] DELPHI Collaboration, *Search for supersymmetric particles in scenarios with a gravitino LSP and stau NLSP*, Eur.Phys.J. C **16** (2000) 211–228, `arXiv:hep-ph/0103026`.

[34] L3 Collaboration, *Search for scalar leptons and scalar quarks at LEP*, Phys.Lett. B **580** (2003) 37–49, `arXiv:hep-ph/0310007`.

[35] OPAL Collaboration, *Search for anomalous production of dilepton events with missing transverse momentum in e^+e^- collisions at $\sqrt{s}$ = 183 Gev to 209 GeV*, Eur.Phys.J. C **32** (2004) 453–473, `arXiv:hep-ph/0309014`.

[36] T. Gleisberg et al., *Event generation with SHERPA 1.1*, JHEP **02** (2009) 007, `arXiv:0811.4622 [hep-ex]`.

[37] J. Alwall et al., *MadGraph/MadEvent v4: The New Web Generation*, JHEP **09** (2007) 028, arXiv:0706.2334 [hep-ph].

[38] T. Sjöstrand, S. Mrenna, and P. Z. Skands, *PYTHIA 6.4 Physics and Manual*, JHEP **0605** (2006) 026, arXiv:hep-ph/0603175.

[39] S. Frixione and B. R. Webber, *Matching NLO QCD computations and parton shower simulations*, JHEP **06** (2002) 029, arXiv:hep-ph/0204244.

[40] B. P. Kersevan and E. Richter-Was, *The Monte Carlo event generator AcerMC version 2.0 with interfaces to PYTHIA 6.2 and HERWIG 6.5*, arXiv:0405247 [hep-ph].

[41] H.-L. Lai et al., *New parton distributions for collider physics*, Phys. Rev. **D82** (2010) 074024, arXiv:1007.2241 [hep-ph].

[42] J. Pumplin et al., *New generation of parton distributions with uncertainties from global QCD analysis*, JHEP **07** (2002) 012, arXiv:hep-ph/0201195.

[43] S. C. et al., *Vector boson production at hadron colliders: A Fully exclusive QCD calculation at NNLO*, Phys. Rev. Lett. **103** (2009) 082001, arXiv:0903.2120 [hep-ex].

[44] A. Martin, W. Stirling, R. Thorne, G. Watt, *Update of parton distributions at NNLO*, Phys. Lett. **B652** (2007) 292, arXiv:0706.0459 [hep-ex].

[45] M. Aliev, H. Lacker, U. Langenfeld, S. Moch and P. Uwer, *HATHOR: HAdronic Top and Heavy quarks cross section calculator*, Comput. Phys. Commun. **182** (2011) 1034, arXiv:1007.1327 [hep-ph].

[46] J. M. Campbell and R. K. Ellis, *An Update on vector boson pair production at hadron colliders*, Phys. Rev. **D60** (1999) 113006, arXiv:hep-ph/9905386 [hep-ph].

[47] J. M. Campbell and R. K. Ellis, *$t\bar{t}W^{\pm}$ production and decay at NLO*, arXiv:1204.5678 [hep-ph].

[48] M. V. Garzelli, A. Kardos, C. G. Papadopoulos, and Z. Trócsányi, *Z^0-boson production in association with a $t\bar{t}$ pair at next-to-leading order accuracy with parton shower effects*, Phys. Rev. **D85** (2012) 074022, arXiv:1111.1444 [hep-ex].

[49] M. B. et. al., *Herwig++ Physics and Manual*, Eur. Phys. J. **C58** (2008) 639–707, arXiv:0803.0883 [hep-ex].

[50] H. B. F.E. Paige, S.D. Protopopescu and X. Tata, *ISAJET: A Monte Carlo event generator for pp, $p\bar{p}$, and e^+e^- reactions*, arXiv:hep-ph/0312045.

[51] W. Beenakker, R. Hopker, M. Spira, and P. Zerwas, *Squark and gluino production at hadron colliders*, Nucl. Phys. **B492** (1997) 51–103, arXiv:hep-ph/9610490.

[52] ATLAS Collaboration, *The ATLAS Simulation Infrastructure*, Eur. Phys. J. **C70** (2010) 823–874, arXiv:1005.4568 [physics.ins-det].

[53] S. Agostinelli et al., *GEANT4: A simulation toolkit*, Nucl. Instrum. Meth. **A506** (2003) 250–303.

[54] ATLAS Collaboration, *The ATLAS Experiment at the CERN Large Hadron Collider*, JINST **3** (2008) S08003.

[55] M. Cacciari, G. P. Salam, and G. Soyez, *The anti-k_t jet clustering algorithm*, JHEP **04** (2008) 063, arXiv:0802.1189 [hep-ph].

[56] M. Cacciari and G. P. Salam, *Dispelling the N^3 myth for the k_t jet-finder*, Phys. Lett. **B641** (2006) 57–61, arXiv:hep-ph/0512210.

[57] ATLAS Collaboration, *Jet energy measurement with the ATLAS detector in proton-proton collisions at $\sqrt{s}$ = 7 TeV*, accepted by Eur. Phys. J. C , arXiv:1112.6426 [hep-ex].

[58] ATLAS Collaboration, *Measurement of the b-tag Efficiency in a Sample of Jets containing Muons with 5 fb^{-1} of Data from the ATLAS Detector*, ATLAS-CONF-2012-043. http://cdsweb.cern.ch/record/1435197.

[59] ATLAS Collaboration, *Determination of the tau energy scale and the associated systematic uncertainty in proton-proton collisions at $\sqrt{s}$ = 7 TeV with the ATLAS detector at the LHC in 2011*, ATLAS-CONF-2012-054. http://cdsweb.cern.ch/record/1342551.

[60] ATLAS Collaboration, *Performance of the Reconstruction and Identification of Hadronic Tau Decays with ATLAS*, ATLAS-CONF-2011-152. http://cdsweb.cern.ch/record/1493491.

[61] ATLAS Collaboration, *Electron performance measurements with the ATLAS detector using the 2010 LHC proton-proton collision data*, Eur. Phys. J. **C72** (2012) 1909, arXiv:1110.3174 [hep-ex].

[62] ATLAS Collaboration, *Muon reconstruction efficiency in reprocessed 2010 LHC proton-proton collision data recorded with the ATLAS detector*, ATLAS-CONF-2011-063. http://cdsweb.cern.ch/record/1345743.

[63] ATLAS Collaboration, *A measurement of the ATLAS muon reconstruction and trigger efficiency using J/psi decays*, ATLAS-CONF-2011-021. http://cdsweb.cern.ch/record/1336750.

[64] ATLAS Collaboration, *Performance of Missing Transverse Momentum Reconstruction in Proton-Proton Collisions at 7 TeV with ATLAS*, Eur. Phys. J. **C72** (2012) 1844, arXiv:1108.5602 [hep-ex].

[65] G. Corcella et al., *HERWIG 6: An Event generator for hadron emission reactions with interfering gluons (including supersymmetric processes)*, JHEP **0101** (2001) 010, arXiv:hep-ph/0011363 [hep-ph].

[66] Mangano, M. L. and Moretti, M. and Piccinini, F. and Pittau, R. and Polosa, A. D., *ALPGEN, a generator for hard multiparton processes in hadronic collisions*, JHEP **0307** (2003) 001, arXiv:hep-ph/0206293 [hep-ph].

[67] S. Frixion, P. Nason, and C. Oleari, *Matching NLO QCD computations with Parton Shower similations: the POWHEG method*, JHEP **11** (2007) 070, arXiv:0709.2092 [hep-ex].

[68] ATLAS Collaboration, *Improved luminosity determination in pp collisions at $\sqrt{s}$ = 7 TeV using the ATLAS detector at the LHC*, submitted to Eur. Phys. J. C, arXiv:1302.4393 [hep-ph].

[69] J. Alwall et al., *Comparative study of various algorithms for the merging of parton showers and matrix elements in hadronic collisions*, Eur. Phys. J. C **53** (2008) 473.

[70] C. W. J. M. Campbell, R. K. Ellis, *Vector boson pair production at the LHC*, JHEP **1107** (2011) 018, arXiv:1105.0020 [hep-ex].

[71] A. L. Read, *Presentation of search results: the CLs technique*, J. Phys. G **28 2693** (2002) .

A Additional plots

The exclusion limits for the OS-m_{T2} (a) and the OS-m_{T2}-nobjet (b) SR are shown in Figure 8 for the Simplified Model with chargino-neutralino production, in Figure 9 for the Simplified Model with chargino-chargino production, and in Figure 10 for the pMSSM model together with observed upper limits on the model cross section (per grid point).

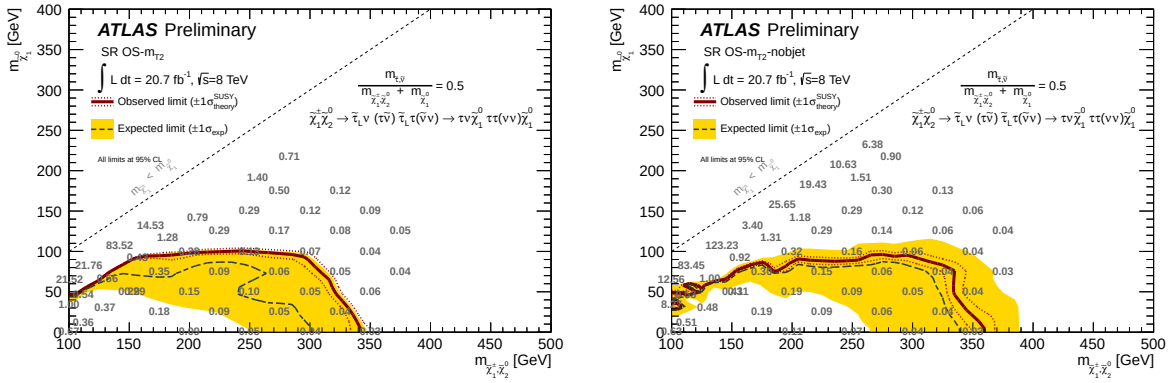

(a) SR OS-m_{T2}

(b) SR OS-m_{T2}-nobjet

Figure 8: 95% CL exclusion limits for a Simplified Model with chargino-neutralino production, for the SR OS-m_{T2} (a) and the SR OS-m_{T2}-nobjet (b). The dashed lines show the 95% CL expected limits. The solid band around the expected limit shows the $\pm 1\sigma$ result where all uncertainties, except those on the signal cross-sections, are considered. The $\pm 1\sigma$ lines around the observed limit represent the results obtained when moving the nominal signal cross-section up and down by the $\pm 1\sigma$ theoretical uncertainty. The overlaid numbers give the observed upper limit on the signal cross section, in pb.

The signal regions used to produce the combined exclusion limits (for each point, the SR with best expected p-value) for all the signal models considered in this document are shown in in Figure 11.

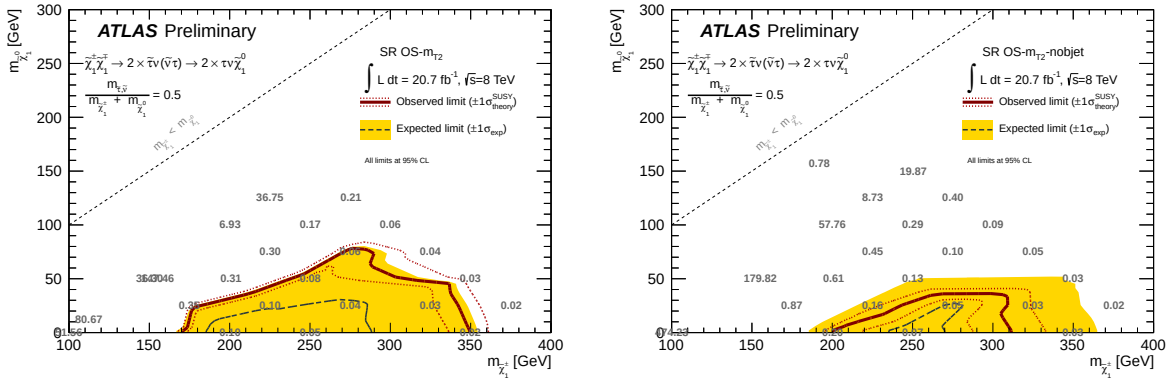

(a) SR OS-m_{T2} (b) SR OS-m_{T2}-nobjet

Figure 9: 95% CL exclusion limits for a Simplified Model with chargino-chargino production, for the SR OS-m_{T2} (a) and the SR OS-m_{T2}-nobjet (b). The dashed lines show the 95% CL expected limits. The solid band around the expected limit shows the $\pm 1\sigma$ result where all uncertainties, except those on the signal cross-sections, are considered. The $\pm 1\sigma$ lines around the observed limit represent the results obtained when moving the nominal signal cross-section up and down by the $\pm 1\sigma$ theoretical uncertainty. The overlaid numbers give the observed upper limit on the signal cross section, in pb.

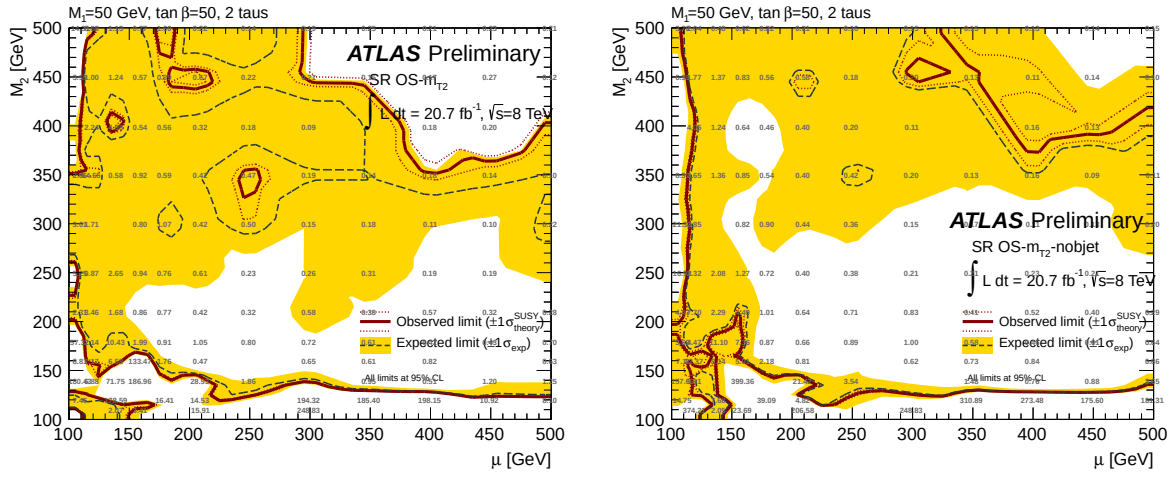

(a) SR OS-m_{T2} (b) SR OS-m_{T2}-nobjet

Figure 10: 95% CL exclusion limits in the pMSSM model for the SR OS-m_{T2} (a) and the SR OS-m_{T2}-nobjet (b). The dashed lines show the 95% CL expected limits. The solid band around the expected limit shows the $\pm 1\sigma$ result where all uncertainties, except those on the signal cross-sections, are considered. The $\pm 1\sigma$ lines around the observed limit represent the results obtained when moving the nominal signal cross-section up and down by the $\pm 1\sigma$ theoretical uncertainty. The overlaid numbers give the observed upper limit on the signal cross section, in pb.

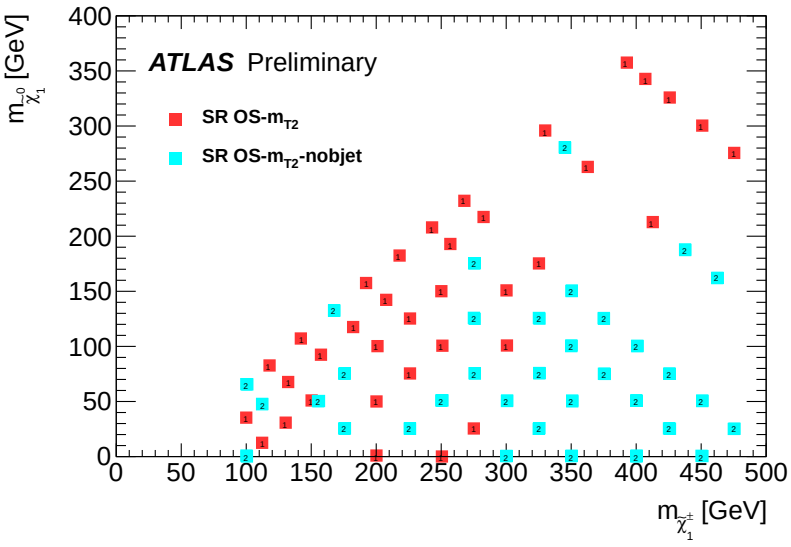

(a) Simplified Model with chargino-neutralino production

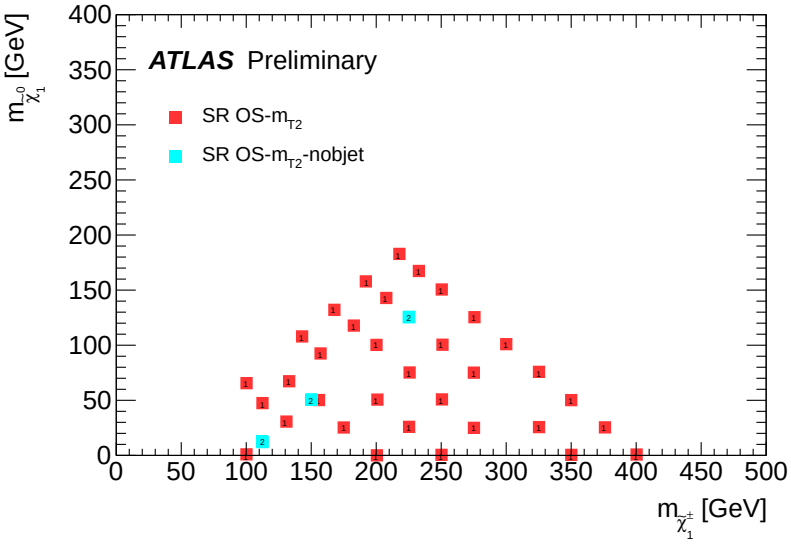

(b) Simplified Model with chargino-chargino production

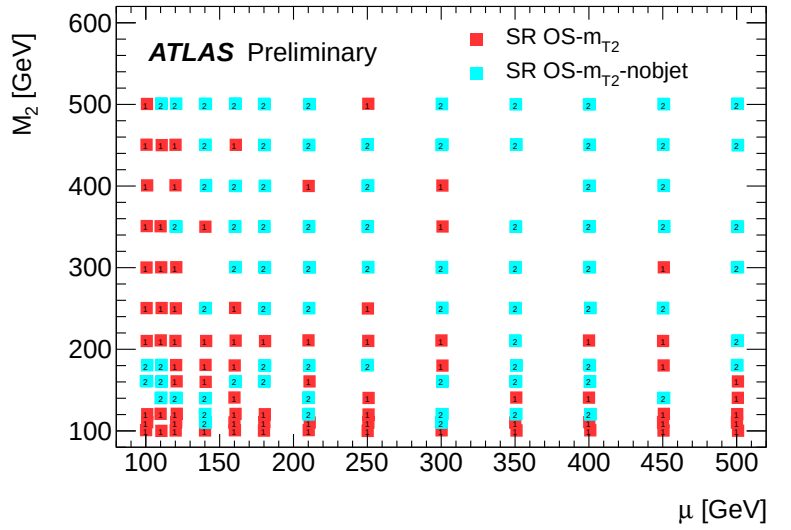

(c) pMSSM

Figure 11: SR with best expected p-value for each point in the Simplified Model with chargino-neutralino production (a), the Simplified Model with chargino-chargino production (b), and in the pMSSM model (c). The SR OS-m_{T2} (OS-m_{T2}-nobjet) is indicated with 1 (2).

B Detailed Cutflows

B.1 Cutflow of benchmark signal points

Selection cut	SUSY Ref. point 1 events ($\mathcal{L}$ =20.7fb^{-1})	SUSY Ref. point 2 events ($\mathcal{L}$ =20.7fb^{-1})
No cuts	2565.7	1852.3
at least 2 leptons (e, μ, τ)	1144.0	581.4
at least 2 τs in the trigger plateau	331.6	212.6
at least 2 τs and trigger	162.9	112.7
at least 2 OS τs	112.1	106.2
jet veto	38.9	54.5
Z-veto	25.6	46.6
$E_{\mathrm{T}}^{\mathrm{miss}}$>40 GeV	21.6	39.1
m_{T2}> 90 GeV	6.8	7.5
Z-veto	59.8	80.4
b-jet veto		
$E_{\mathrm{T}}^{\mathrm{miss}}$>40 GeV	52.2	68.1
m_{T2}> 100 GeV	9.2	8.9

Table 7: Cutflows for the benchmark SUSY points defined in Section 2. The number of simulated events is 20000 (40000) for SUSY Ref. point 1 (SUSY Ref. point 2).